



HAL
open science

Jet-cooled FTIR spectroscopy and analysis of the ν_5 C–O stretch fundamental of Ni(CO)₄

Vincent Boudon, Pierre Asselin, Pascale Soulard

► **To cite this version:**

Vincent Boudon, Pierre Asselin, Pascale Soulard. Jet-cooled FTIR spectroscopy and analysis of the ν_5 C–O stretch fundamental of Ni(CO)₄. *Molecular Physics*, 2008, A Special Issue on High Resolution Molecular Spectroscopy–Dijon 2007, 106 (09-10), pp.1135-1141. 10.1080/00268970701765795. hal-00513161

HAL Id: hal-00513161

<https://hal.science/hal-00513161v1>

Submitted on 1 Sep 2010

HAL is a multi-disciplinary open access archive for the deposit and dissemination of scientific research documents, whether they are published or not. The documents may come from teaching and research institutions in France or abroad, or from public or private research centers.

L'archive ouverte pluridisciplinaire **HAL**, est destinée au dépôt et à la diffusion de documents scientifiques de niveau recherche, publiés ou non, émanant des établissements d'enseignement et de recherche français ou étrangers, des laboratoires publics ou privés.



Jet-cooled FTIR spectroscopy and analysis of the ν_5 C--O stretch fundamental of $\text{Ni}(\text{CO})_4$

Journal:	<i>Molecular Physics</i>
Manuscript ID:	TMPH-2007-0273.R1
Manuscript Type:	Full Paper
Date Submitted by the Author:	04-Oct-2007
Complete List of Authors:	Boudon, Vincent; Chercheur CNRS, ICB Asselin, Pierre; Universit'e Pierre et Marie Curie, LADIR Soulard, Pascale; Universit'e Pierre et Marie Curie, LADIR
Keywords:	Tetracarbonyl, FTIR spectroscopy, Supersonic jet, Spherical-top, Rovibrational analysis
<p>Note: The following files were submitted by the author for peer review, but cannot be converted to PDF. You must view these files (e.g. movies) online.</p> <p>paper.tex tMPH2e.cls upmath.sty cite.sty</p>	



Jet-cooled FTIR spectroscopy and analysis of the ν_5 C–O stretch fundamental of $\text{Ni}(\text{CO})_4$

P. ASSELIN¹, P. SOULARD¹ and V. BOUDON^{2,*}

¹LADIR, CNRS UMR 7075, Université Pierre et Marie Curie,
4 Place Jussieu, Bat. F74, Case 49, F-75252, Paris, France.

²Institut Carnot de Bourgogne - UMR 5209 CNRS-Université de Bourgogne,
9, av. Alain Savary, B.P. 47870, F-21078 Dijon Cedex, France.

(00 Month 200x; In final form 00 Month 200x)

Rovibrational spectra of the C–O stretch band (ν_5) of $\text{Ni}(\text{CO})_4$ have been recorded at 0.006 cm^{-1} resolution by coupling a low pressure continuous supersonic jet with a high resolution interferometer.

The spectrum has been analyzed thanks to the STDS software (see <http://icb.u-bourgogne.fr/OMR/SMA/SHTDS/>) that implements the tensorial formalism developed in the Dijon group for tetrahedral molecules. We obtain a very satisfying simulation thanks to an effective Hamiltonian expanded up to order 3. The asymmetry of the high- J lines is due to a small tetrahedral splitting and is well reproduced. The root mean square deviation is $0.96 \times 10^{-3} \text{ cm}^{-1}$. The Coriolis constant is somewhat larger than for other spherical-top carbonyls like $\text{Mo}(\text{CO})_6$ and $\text{W}(\text{CO})_6$ and, as a consequence, the level structure displays a standard three-branch structure, typical for triply degenerate fundamentals.

Keywords: Tetracarbonyl, FTIR spectroscopy, Supersonic jet, Spherical-top, Rovibrational analysis, Tensorial formalism, Semi-classical analysis.

1 Introduction

Four transition-metal carbonyls are spherical-top molecules. Three are octahedral: $\text{Cr}(\text{CO})_6$ [1], $\text{Mo}(\text{CO})_6$ [2] and $\text{W}(\text{CO})_6$ [3], while one is tetrahedral, namely $\text{Ni}(\text{CO})_4$. Some years ago, the nickel hexacarbonyl infrared-active C–O stretch fundamental (ν_5) was investigated at high-resolution using a supersonic expansion jet by Davies and co-workers [4, 5]. A similar work was performed recently on non-tetrahedral C and O isotopic substitutions by Martinez and Morse [6].

The papers of Davies *et al.*, however, only report on harmonic frequencies and rotational constants. No other rovibrational constant (Coriolis coupling, tetrahedral splitting, ...) was determined. Moreover, in Ref. [5], rotational constants on both the ground and $v_5 = 1$ states are simultaneously fitted, while the Coriolis constant is fixed to zero. For a triply degenerate fundamental of a spherical-top, this is not correct, because there is necessarily a non-zero (even if it is small) Coriolis constant. It is not possible to determine it simultaneously with the ground and excited state rotational constants using only excited state data. The access to precise values of Coriolis constants can also be very useful to derive internuclear distances by taking advantage of real B_0 values determined for at least two tetrahedral isotopologues in the case of $\text{Ni}(\text{CO})_4$.

We have thus decided to reinvestigate this band thanks to a new jet-cooled FTIR spectrum. For the analysis, we use here the electron-diffraction value for the ground state rotational constant B_0 and we fit the excited state rovibrational constants up to order 3. The Coriolis constant is shown to be small, but somewhat larger than in the case of $\text{Mo}(\text{CO})_6$ [2] and $\text{W}(\text{CO})_6$ [3]. Although it is very small, we show that the tetrahedral splitting can be observed and the corresponding parameters can be determined. We also discuss briefly the semi-classical description of the rovibrational energy levels, as it was done (although in a more detailed way since this was a particular case) for $\text{Mo}(\text{CO})_6$ in Ref. [7].

*Corresponding author. Email: Vincent.Boudon@u-bourgogne.fr

2 Experiment

The low pressure supersonic jet-FTIR spectrometer set-up at LADIR has been described in details elsewhere [2]. Briefly, Ni(CO)₄ obtained from Strem (> 98 % purity) is seeded in argon at about 20 % by bubbling the rare gas through the liquid metal carbonyl into a constantly cooled bath maintained at about -60°C. The 1 mol.h⁻¹ flow rate of the Ni(CO)₄/Ar gas mixture is expanded at a stagnation pressure of 80 mbar through a 0.74 mm circular nozzle into a vacuum chamber evacuated at a background pressure of 10⁻³ mbar by a 18 m³.h⁻¹ Varian four stage oil diffusion pump backed by a 400 m³.h⁻¹ roots pump (Edwards 500 H) and a 60 m³.h⁻¹ rotary vane pump (Leybold D60). The supersonic expansion is finally probed by the 16-pass arrangement of the IR beam issued from a Bruker IFS 120 HR interferometer and then focused on a InSb detector equipped with a narrow bandpass filter centered around the C–O stretching region (1950-2100 cm⁻¹). A typical jet spectrum of the ν_5 stretching band of Ni(CO)₄ represents the Fourier transform of 10 coadded interferograms recorded at 0.006 cm⁻¹ resolution. Particularly concentrated Ni(CO)₄/Ar mixtures have been used in the present work to obtain a higher rotational temperature T_r (25 K from our rovibrational band contour simulations) which enables to observe higher J transitions containing tetrahedral splitting information.

3 Theory

Ni(CO)₄ possesses nine normal modes of vibration [8]: 2 non-degenerate modes with A_1 symmetry (ν_1 and ν_2), 2 doubly-degenerate modes with E symmetry (ν_3 and ν_4), one triply-degenerate mode with F_1 symmetry (ν_9) and 4 triply-degenerate modes with F_2 symmetry (ν_5 , ν_6 , ν_7 and ν_8). Only F_2 fundamentals are infrared active. ν_5 corresponds to a C–O stretch mode.

Since both the ¹²C and ¹⁶O atoms have a zero nuclear spin, the spin statistical weights of Ni(¹²C¹⁶O)₄ are such that only levels with A_1 or A_2 rovibrational symmetry species are allowed (in this work, we only considered this main isotopologue, the others being not observed under the present experimental conditions).

The theoretical model described below to develop the Hamiltonian operator is based on the tensorial formalism and vibrational extrapolation methods used in Dijon. These methods have already been explained for example in Ref. [9]. We only recall here the basic principles and their application to the case of a tetrahedral molecule.

If we consider an X(YZ)₄ molecule for which the vibrational levels are grouped in a series of polyads designed by P_k ($k = 0, \dots, n$), P_0 being the ground state (GS), the Hamiltonian operator can be put in the following form (after performing some contact transformations) :

$$\mathcal{H} = \mathcal{H}_{\{P_0 \equiv \text{GS}\}} + \mathcal{H}_{\{P_1\}} + \dots + \mathcal{H}_{\{P_k\}} + \dots + \mathcal{H}_{\{P_{n-1}\}} + \mathcal{H}_{\{P_n\}}. \quad (1)$$

Terms like $\mathcal{H}_{\{P_k\}}$ contain rovibrational operators which have no matrix elements within the $P_{k' > k}$ basis sets. The effective Hamiltonian for polyad P_n is obtained by projecting \mathcal{H} in the P_n Hilbert subspace, *i.e.*

$$\begin{aligned} H^{\langle P_n \rangle} &= P^{\langle P_n \rangle} \mathcal{H} P^{\langle P_n \rangle} \\ &= H_{\{\text{GS}\}}^{\langle P_n \rangle} + H_{\{P_1\}}^{\langle P_n \rangle} + \dots + H_{\{P_k\}}^{\langle P_n \rangle} + \dots + H_{\{P_{n-1}\}}^{\langle P_n \rangle} + H_{\{P_n\}}^{\langle P_n \rangle}. \end{aligned} \quad (2)$$

The different terms are written in the form

$$\mathcal{H}_{\{P_k\}} = \sum_{\text{all indexes}} t_{\{s\}\{s'\}}^{\Omega(K,n\Gamma)\Gamma_v\Gamma'_v} \beta \left[\varepsilon V_{\{s\}\{s'\}}^{\Omega_v(\Gamma_v\Gamma'_v)\Gamma} \otimes R^{\Omega(K,n\Gamma)} \right]^{(A_1)}. \quad (3)$$

In this equation, the $t_{\{s\}\{s'\}}^{\Omega(K,n\Gamma)\Gamma_v\Gamma'_v}$ are the parameters to be determined, while $\varepsilon V_{\{s\}\{s'\}}^{\Omega_v(\Gamma_v\Gamma'_v)\Gamma}$ and $R^{\Omega(K,n\Gamma)}$ are vibrational and rotational operators of respective degree Ω_v and Ω . Their construction is described in Ref. [9]. Again, the vibrational operators only have matrix elements within the $P_{k' \leq k}$ basis sets. β is a

factor that allows the scalar terms ($\Gamma = A_1$) to match the usual terms like $B_0 J^2$, *etc.* The order of each individual term is $\Omega + \Omega_v - 2$.

Such a Hamiltonian development scheme enables the treatment of any polyad system. In this work however, since we only consider an isolated fundamental band, we will use only the two following effective Hamiltonians :

- The ground state (GS) effective Hamiltonian,

$$H^{<GS>} = H_{\{GS\}}^{<GS>} . \quad (4)$$

- The ν_5 C–O stretch fundamental effective Hamiltonian,

$$H^{<\nu_5>} = H_{\{GS\}}^{<\nu_5>} + H_{\{\nu_5\}}^{<\nu_5>} . \quad (5)$$

A dipole moment operator is developed in the same way (see for instance [9] for details about its construction).

We use here a vibrational basis restricted to the ν_5 mode:

$$\left| \Psi_v^{(C_v)} \right\rangle = \left| \Psi_{v_5=1}^{(l_5=1, F_2)} \right\rangle , \quad (6)$$

i.e. we use a harmonic oscillator wavefunction for a triply degenerate fundamental with vibrational angular momentum l_5 . The Hamiltonian and dipole moment matrix elements are calculated in the coupled rovibrational basis

$$\left[\left[\Psi_v^{(C_v)} \otimes \Psi_r^{(J, n C_r)} \right] (C) \right\rangle , \quad (7)$$

$\Psi_r^{(J, n C_r)}$ being a rotational wavefunction with angular momentum J , rotational symmetry species C_r and multiplicity index n (see [9]) and C the overall symmetry species ($C = C_v \otimes C_r$).

4 Analysis

The ground state rotational constants of $Ni(CO)_4$ are not known in detail. We thus expand $H^{<GS>}$ up to order zero only, which implies only one parameter, that is the ground-state rotational constant $t_{\{000000000F_2\}\{000000000A_1\}}^{2(0,0A_1)A_1A_1} = B_0$. If we use the electron diffraction bond lengths of Hedberg *et al.* [8], namely $r_{Ni-C} = 1.838(2)$ Å and $r_{C=O} = 1.141(2)$ Å, we can calculate an approximate B_0 value. We get:

$$B_0 = \frac{3\hbar}{32\pi c \left(m_C r_{Ni-C}^2 + m_O (r_{Ni-C} + r_{C=O})^2 \right)} \simeq 0.0346 \text{ cm}^{-1} . \quad (8)$$

$H^{<\nu_5>}$ is expanded up to order 3. By using the band center of Davies *et al.* [4, 5] and moving by hand the Coriolis constant term $t_{\{000010000F_2\}\{000010000F_2\}}^{1(1,0F_1)F_2F_2}$, we could make some preliminary assignments and fit the scalar terms (those with $\Gamma = A_1$).

To go further, we noticed that the high J lines, which in fact correspond to clusters of many lines, are slightly asymmetric. We attributed this to a small tetrahedral splitting due to the $t_{\{000010000F_2\}\{000010000F_2\}}^{3(1,0F_1)F_2F_2}$ anisotropic Coriolis term. By moving this value by hand, we could assign some lines to peak positions obtained by fitting Gaussian shapes to the experimental data, as illustrated on Figure 1.

[Insert Figure 1 about here.]

It is then possible to fit 6 effective Hamiltonian parameters. The results are given in Table 1. Since the Q branch is too congested to be experimentally resolved, no Q line could be assigned. As it is usual in this case, for an unperturbed triply degenerate fundamental of a spherical-top, the $t_{\{000010000F_2\}}^{2(2,0E)F_2F_2}$ and $t_{\{000010000F_2\}}^{2(2,0F_2)F_2F_2}$ parameters cannot be fitted simultaneously. Thus it is necessary to fix one of them. But the value to which it is fixed has a strong influence on the Q branch shape. We thus chose to move $t_{\{000010000F_2\}}^{2(2,0F_2)F_2F_2}$ by hand (and fit the other parameters) until this shape was consistent with the experimental spectrum. Then, we kept the value obtained in this way.

Figure 2 shows an overview of the experimental spectrum, compared to the simulation. One distinguishes somewhat intense broad bands on the low wavenumber side of the Q branch. According to the work of Davies *et al.* [5] these features are assignable to the Q branches of hot bands starting from two low frequency C–Ni–C bending vibrations, namely ν_4 (62 cm^{-1}) and ν_8 (79 cm^{-1}). The intensity ratio, of about respectively 18 % and 12 % between these hot bands and the ν_5 fundamental band provides an estimate of the vibrational temperature (T_v) in the jet, that is about 50 K. The important difference observed between T_v and T_r originates in the more efficient rotational relaxation in the supersonic expansion. Figure 3 displays a small portion of the R branch from the same experimental spectrum.

[Insert Figure 2 about here.]

[Insert Figure 3 about here.]

[Insert Figure 4 about here.]

[Insert Table 1 about here.]

Concerning transition intensities, the dipole moment operator has been expanded up to order 1. Since no absolute measurement of the line strengths is available, the order zero parameter (which is the dipole moment derivative relative to the ν_5 mode) was simply set to one. In order to match the experimental relative intensity ratio between P and R lines, we used the first order parameter (which is a so-called Herman-Wallis factor). This one was set to the value given in Table 1.

5 Discussion

As a first remark, although we have used here natural abundance nickel which contains five different isotopes (^{58}Ni : 68.077 %, ^{60}Ni : 26.223 %, ^{61}Ni : 1.140 %, ^{62}Ni : 3.634 %, ^{64}Ni : 0.926 %), we observe no isotopic shift. This is usual for carbonyl molecules, for which the C–O stretch modes are not affected by isotopic substitutions of the metal atom [2, 3].

Another interesting point is related to the comparison of the value of the Coriolis parameter between different carbonyls. We can calculate an approximate value of the ζ_5 Coriolis constant, that is

$$\zeta_5 \simeq \frac{t_{\{000010000F_2\}}^{1(1,0F_1)F_2F_2}}{3\sqrt{2}B_0} \simeq -0.032. \quad (9)$$

This value is somewhat larger than that reported by Hedberg *et al.* [8] (-0.02), but the order of magnitude is consistent. Such a value is small, but it is one order of magnitude larger than is the case of the ν_6 C–O stretch fundamental of octahedral hexacarbonyls like $\text{Mo}(\text{CO})_6$ ($\zeta_6 \simeq -0.0044$ [2]) and $\text{W}(\text{CO})_6$ ($\zeta_6 \simeq 0.0023$ [3]). Thus, we do not expect here the same striking level exchange phenomena as those observed in $\text{Mo}(\text{CO})_6$ [7] since a larger Coriolis constant better separates the branches.

We can notice that the value of B_0 given in Table II of Ref. [5] is in fact an effective value,

$$\tilde{B}_0 \simeq B_0(1 - \zeta_5) \simeq 0.0357213 \text{ cm}^{-1}, \quad (10)$$

(since it was fitted without the Coriolis term). With our ζ_5 value obtained above, we get $B_0 \simeq 0.03462$ cm^{-1} , which is very close to the electron-diffraction value and this fully justifies our initial approximation.

To illustrate the effect of the Coriolis constant, the calculated reduced energy levels for the ν_5 band are displayed on Figure 5. The reduced energy levels are obtained by subtracting the scalar term, *i.e.*,

$$\begin{aligned} E_{\text{red}} &= E - \sum_{\Omega} t_{\{000000000\}\{000000000\}}^{\Omega(0,0A_1)A_1A_1} (J(J+1))^{\Omega/2} \\ &= E - B_0 J(J+1) + D_0 J^2 (J+1)^2 - \dots \end{aligned} \quad (11)$$

We remark that the levels are distributed among three well separated branches even for low J values. This is not the case for $\text{Mo}(\text{CO})_6$ because the Coriolis constant is one order of magnitude smaller.

On the same Figure, we plotted the semiclassical energy curves obtained in the same way as in Ref. [7]. Let us simply recall that in this model, the quantum description of the vibrational part of the Hamiltonian is combined with the classical description of the rotational degrees of freedom. Using the vibrational basis functions

$$\{|v_{5x}, v_{5y}, v_{5z}\rangle\} = \{|1, 0, 0\rangle, |0, 1, 0\rangle, |0, 0, 1\rangle\}, \quad (12)$$

we get the following matrix of the effective Hamiltonian :

$$\hat{H} = \begin{pmatrix} H_{11} & H_{21}^* & H_{31}^* \\ H_{21} & H_{22} & H_{32}^* \\ H_{31} & H_{32} & H_{33} \end{pmatrix}, \quad (13)$$

where the different terms are expressed in terms of the rotational angular momentum components (J_x , J_y , J_z). Detailed expressions can be found in Ref. [7]. The rotational operators J_x , J_y , and J_z are then converted to classical dynamical variables

$$(J_x, J_y, J_z) = \mathcal{J}(\sin \theta \cos \phi, \sin \theta \sin \phi, \cos \theta), \quad (14)$$

where angles ϕ and θ define the axis of rotation and \mathcal{J} is the constant amplitude of the classical angular momentum,

$$\mathcal{J} = \sqrt{J(J+1)}. \quad (15)$$

The angles (θ, ϕ) are the coordinates on the classical phase space for the rotational motion, called rotational *phase sphere* [11–14]. Diagonalization of matrix (13) for a given value of \mathcal{J} and for each direction (θ, ϕ) gives three eigenvalues $E_k^{\mathcal{J}}(\theta, \phi)$ ($k = -1, 0$ and $+1$) which represent three classical rotational energy surfaces defined as functions on the rotational phase sphere. We are particularly interested in the values of $E_k^{\mathcal{J}}(\theta, \phi)$ for stationary axes of rotation. Principal stationary axes of any T_d spherical-top molecule are its symmetry axes C_4 , C_3 , and C_2 . The T_d group has several axes of each kind equivalent by symmetry and naturally the value of $E_k^{\mathcal{J}}$ for each of the equivalent axes is the same. More precisely, equivalent by symmetry points (θ, ϕ) form an orbit of *equivalent* points on the rotational phase sphere. The principal axes are *always* stationary, and moreover, axes C_4 and C_3 should be stable for any generic Hamiltonian. This means that generically functions $E_k^{\mathcal{J}}$ have a nondegenerate maximum, a minimum, or a saddle at the corresponding points on the phase sphere for any J . These points form *critical orbits* [15] with local symmetry C_2 , C_3 , and C_4 . The C_4 and C_3 points can either be a maximum or a minimum, while the C_2 point can also be a saddle. To calculate $E_k^{\mathcal{J}}$ we choose one representative in each critical orbit indicated in Table 2. Simple analytical expressions can be found for the energies on the critical orbits by diagonalizing the matrix (13) and are given in Ref. [7].

[Insert Table 2 about here.]

The curves on Figure 5 perfectly match the quantum energy levels in each branch and never cross, confirming that there is no level exchange between the branches in this case. In other words, we find again the usual splitting of the F_2 vibrational states into three components (corresponding to the three eigenvalues E_k^J defined above) with effective quantum numbers $R = J - 1, J, J + 1$. There is almost no mixing between these components.

[Insert Figure 5 about here.]

6 Conclusion

This work constitutes the first detailed analysis of the ν_5 C–O stretch fundamental of $\text{Ni}(\text{CO})_4$, including the Coriolis constant and non-scalar terms that induce tetrahedral splitting. We have also shown that, contrary to spherical-top hexacarbonyls $\text{Mo}(\text{CO})_6$ and $\text{W}(\text{CO})_6$, tetrahedral $\text{Ni}(\text{CO})_4$ has a C–O stretch fundamental with a standard Coriolis structure.

The present analysis was performed thanks to the STDS set of programs [16] that implements the Dijon tensorial formalism methods [9, 17] and which is freely available at the URL <http://icb.u-bourgogne.fr/OMR/SMA/SHTDS/>.

Acknowledgments

Support from the Région Bourgogne for the computer equipment of the Institut Carnot de Bourgogne is gratefully acknowledged. We also wish to thank the SpecMo network of the CNRS.

References

- [1] G. Hansford and P. Davies, *J. Mol. Spectrosc.* **168**, 540 (1994).
- [2] P. Asselin, P. Soulard, L. Manceron, V. Boudon, and G. Pierre, *J. Mol. Struct.* **517**, 145 (2000).
- [3] G. Hansford, M. Loroño, and P. Davies, *J. Chem. Phys.* **112**, 3620 (2000).
- [4] P. B. Davies, N. A. Martin, M. D. Nunes, D. A. Pape, and D. K. Russel, *Chem. Phys. Lett.* **156**, 553 (1989).
- [5] P. B. Davies, N. A. Martin, M. D. Nunes, D. A. Pape, and D. K. Russel, *J. Chem. Phys.* **90**, 1576 (1990).
- [6] A. Martinez and M. D. Morse, *J. Chem. Phys.* **124**, 124316 (2006).
- [7] G. Dhont, D. Sadovskii, B. Zhilinskii, and V. Boudon, *J. Mol. Spectrosc.* **201**, 95 (2000).
- [8] L. Hedberg, T. Iijima, and K. Hedberg, *J. Chem. Phys.* **70**, 3224 (1979).
- [9] J.-P. Champion, M. Loëte, and G. Pierre, in *Spectroscopy of the Earth's atmosphere and interstellar medium*, edited by K. N. Rao and A. Weber (Academic Press, San Diego, 1992), pp. 339–422.
- [10] A. Robiette, D. Gray, and F. Birss, *Mol. Phys.* **32**, 1591 (1976).
- [11] W. G. Harter and C. Patterson, *J. Chem. Phys.* **80** (1984).
- [12] W. G. Harter, *Comp. Phys. Rep.* **8**, 319 (1988).
- [13] D. Sadovskii and B. Zhilinskii, *Mol. Phys.* **65**, 109 (1988).
- [14] V. Pavlov-Verevkin, D. Sadovskii, and B. Zhilinskii, *Europhys. Lett.* **6**, 573 (1988).
- [15] L. Michel, *Rev. Mod. Phys.* **52**, 617 (1980).
- [16] C. Wenger and J.-P. Champion, *J. Quant. Spectrosc. Radiat. Transfer* **59**, 471 (1998).
- [17] V. Boudon, J.-P. Champion, T. Gabard, M. Loëte, F. Michelot, G. Pierre, M. Rotger, C. Wenger, and M. Rey, *J. Mol. Spectrosc.* **228**, 620 (2004).

Table 1. Effective Hamiltonian and dipole moment parameters.

<i>Hamiltonian parameters</i>						
Level	Order	Parameter $t_{\Omega(K,n\Gamma)\Gamma_v\Gamma'_v}^{\{s\}\{s'\}}$	Γ_v	Γ'_v	Value/cm ⁻¹	Notation of Robiette <i>et al.</i> [10]
GS	0	2(0, 0A ₁)	000000000A ₁	000000000A ₁	3.46 × 10 ⁻² †	B ₀
ν ₅ = 1	0	0(0, 0A ₁)	000010000F ₂	000010000F ₂	2061.30937(27)	ν ₅
	1	1(1, 0F ₁)	000010000F ₂	000010000F ₂	-4.712(19) × 10 ⁻³	3√2(Bζ) ₅
	2	2(0, 0A ₁)	000010000F ₂	000010000F ₂	-4.794(12) × 10 ⁻⁵	B ₅ - B ₀
		2(2, 0E)	000010000F ₂	000010000F ₂	-8.34(21) × 10 ⁻⁶	-α ₂₂₀ /2 - 6α ₂₂₄
		2(2, 0F ₂)	000010000F ₂	000010000F ₂	-0.5 × 10 ^{-5a}	-3α ₂₂₀ /4 + 6α ₂₂₄
	3	3(1, 0F ₁)	000010000F ₂	000010000F ₂	-2.82(29) × 10 ⁻⁸	-(3√3/4√2)F ₁₁₀
		3(3, 0F ₁)	000010000F ₂	000010000F ₂	9.25(13) × 10 ⁻⁸	(3√5/2)F ₁₃₄
211 data fitted			J _{max} =62		d _{RMS} = 0.957 × 10 ⁻³ cm ⁻¹	
<i>Dipole moment parameters</i>						
Transition	Order	Parameter $\mu_{\Omega(K,n\Gamma)\Gamma_v\Gamma'_v}^{\{s\}\{s'\}}$	Γ_v	Γ'_v	Value/arb. unit	Comments
ν ₅ -GS	0	0(0, 0A ₁)	000000000A ₁	000010000F ₂	1.0 ^a	
	1	1(1, 0F ₁)	000000000A ₁	000010000F ₂	-2.0 × 10 ⁻³ †	Herman-Wallis

^a Fixed parameter (see text).

Table 2. Stationary rotation axes of a tetrahedral molecule.

Axis	$[J_x, J_y, J_z]$	(θ, ϕ)	Number
C_4	$[0, 0, 1]$	$(0, 0)$	3
C_3	$[1, 1, 1]/\sqrt{3}$	$(\arctan \sqrt{2}, \pi/4)$	4
C_2	$[1, 1, 0]/\sqrt{2}$	$(\pi/2, \pi/4)$	6

For Peer Review Only

Figure captions

1
2
3
4
5
6
7
8
9
10
11 Figure 1. Tetrahedral splitting for high J values in the R branch of the ν_5 band of $\text{Ni}(^{12}\text{C}^{16}\text{O})_4$; arrows indicate how assignments
12 were made; vertical sticks show the calculated individual transitions
13

14
15 Figure 2. Overview of the spectrum of the ν_5 band of $\text{Ni}(^{12}\text{C}^{16}\text{O})_4$, compared to the simulation.
16

17
18 Figure 3. Detail in the R branch of the ν_5 band of $\text{Ni}(^{12}\text{C}^{16}\text{O})_4$, compared to the simulation.
19

20
21 Figure 4. Observed–calculated wavenumbers for the ν_5 band of $\text{Ni}(^{12}\text{C}^{16}\text{O})_4$.
22

23
24 Figure 5. Calculated reduced energy levels and semiclassical energy curves (see text) for the ν_5 band of $\text{Ni}(^{12}\text{C}^{16}\text{O})_4$.
25
26
27
28
29
30
31
32
33
34
35
36
37
38
39
40
41
42
43
44
45
46
47
48
49
50
51
52
53
54
55
56
57
58
59
60

Fig. 1

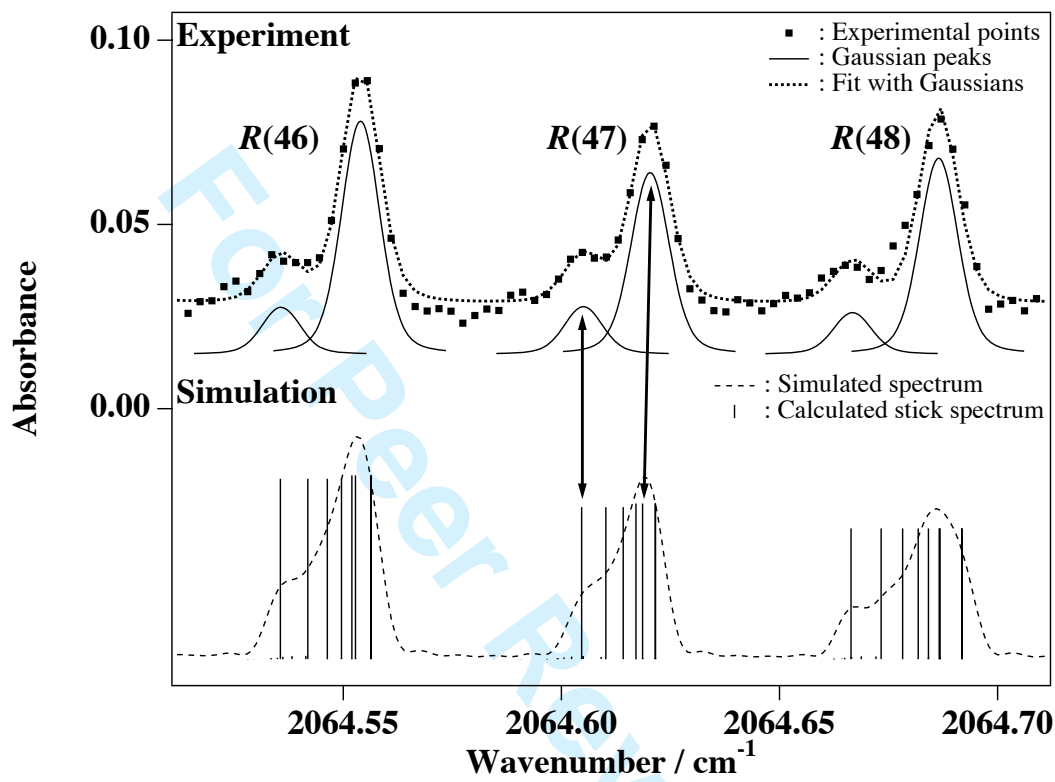


Fig. 2

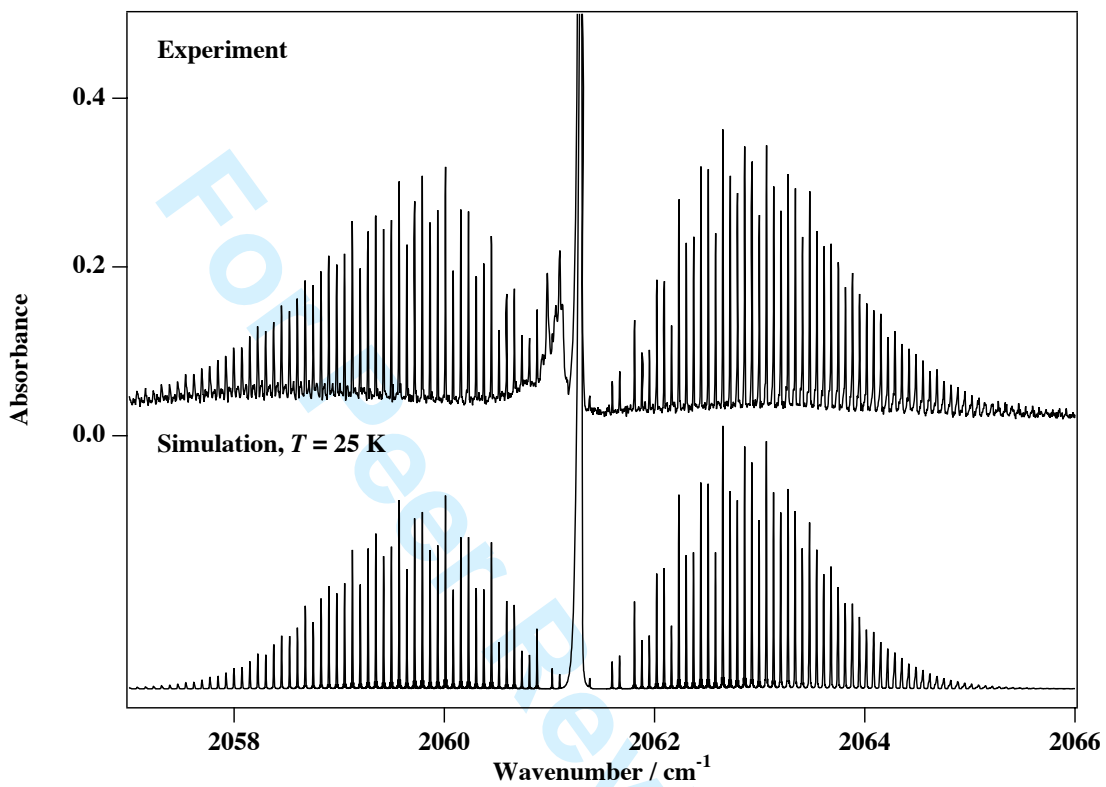


Fig. 3

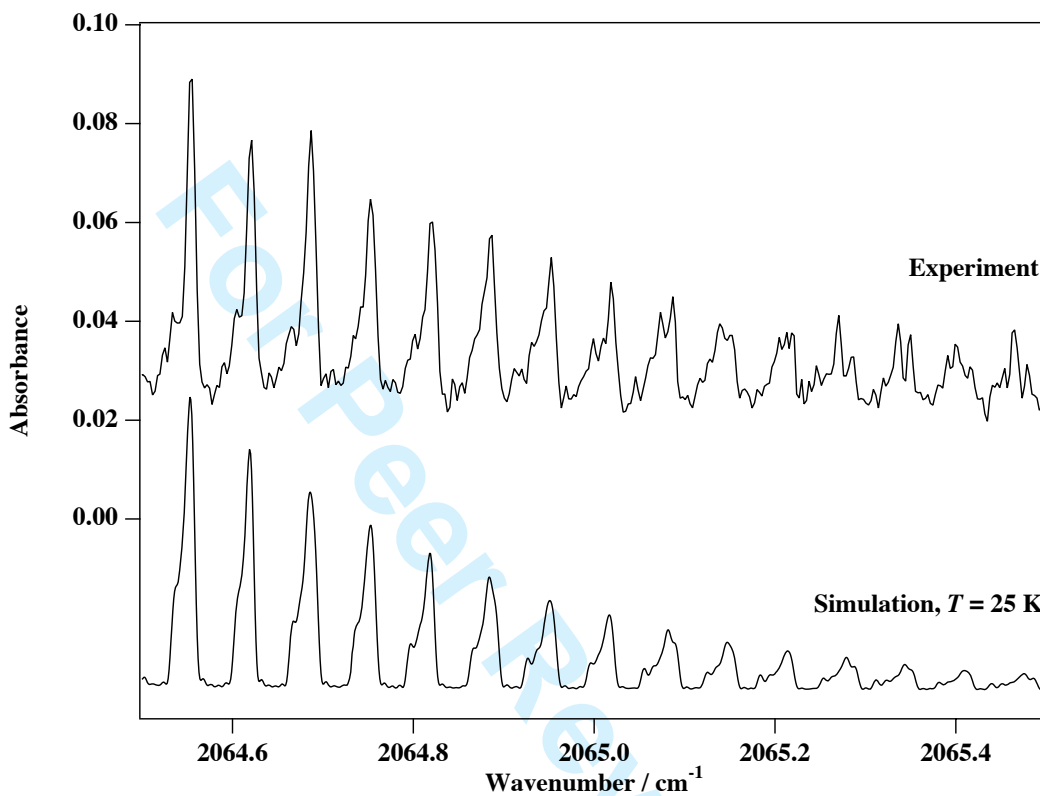


Fig. 4

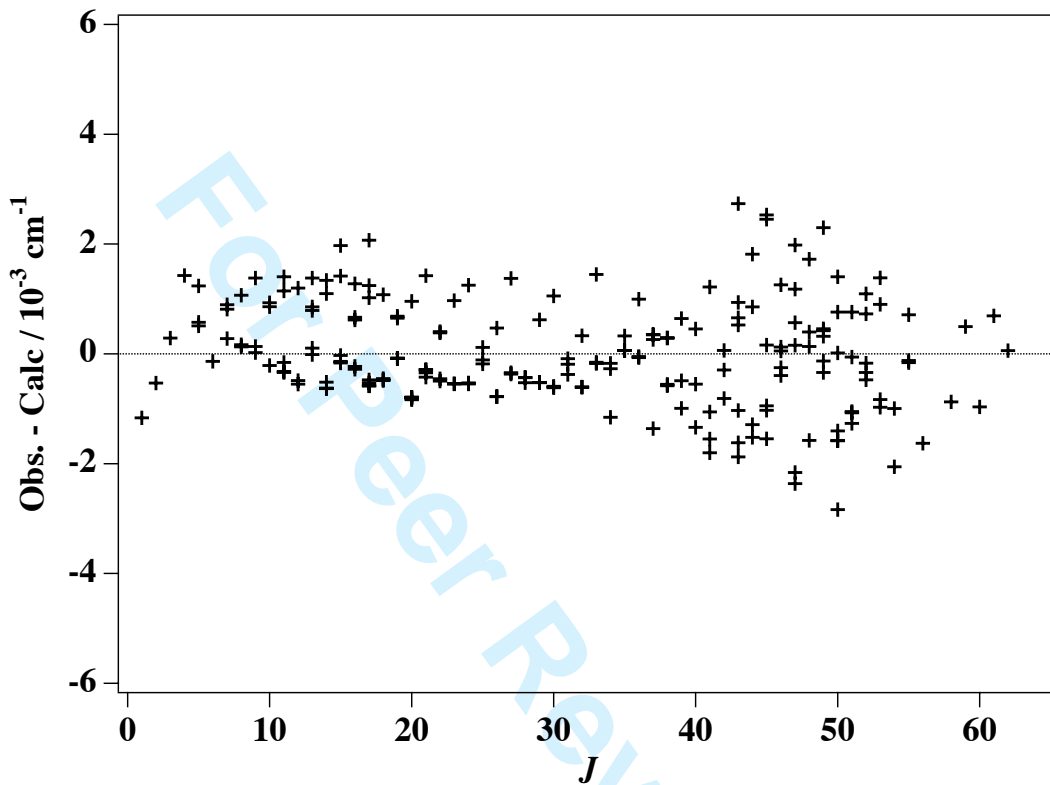
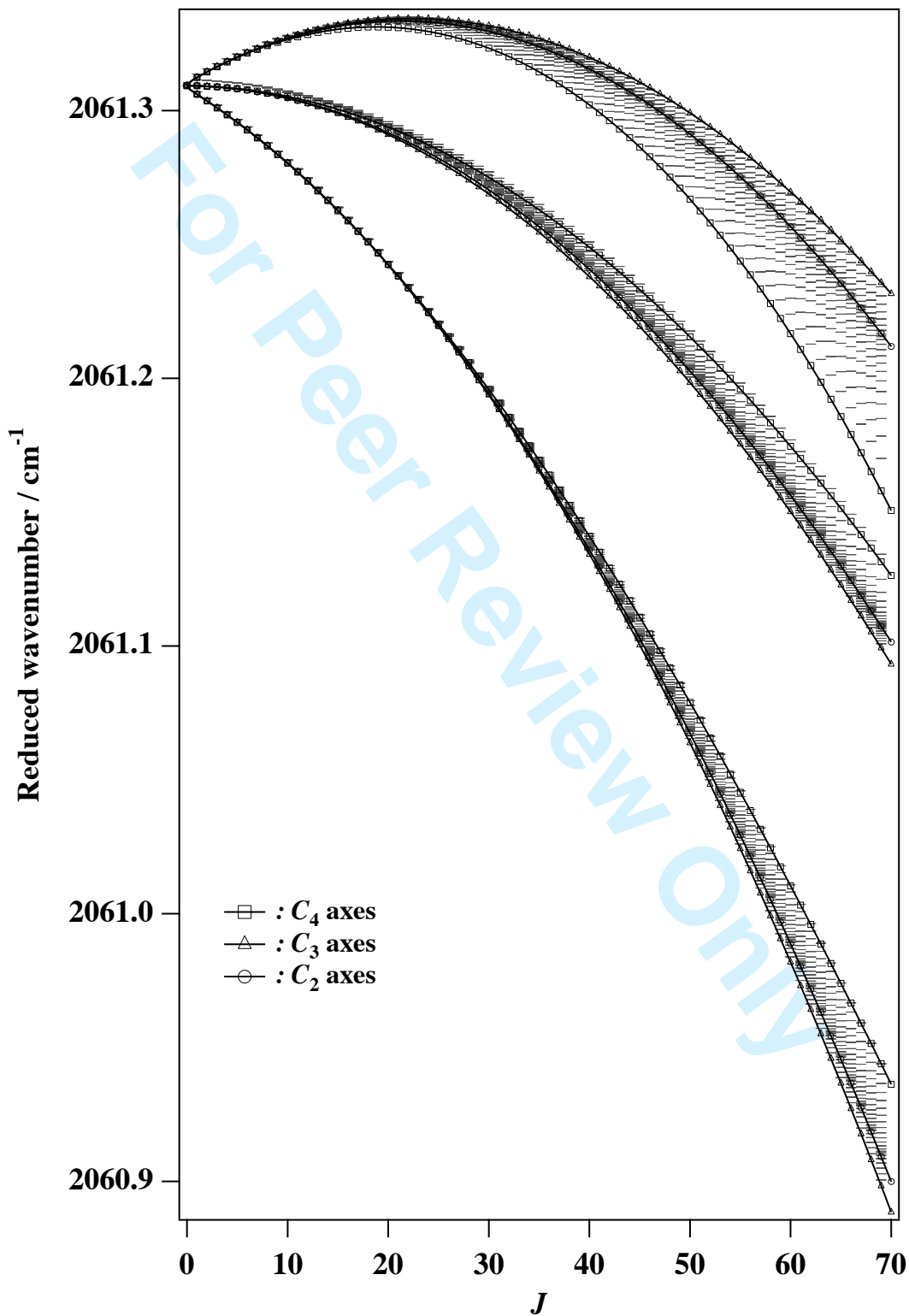
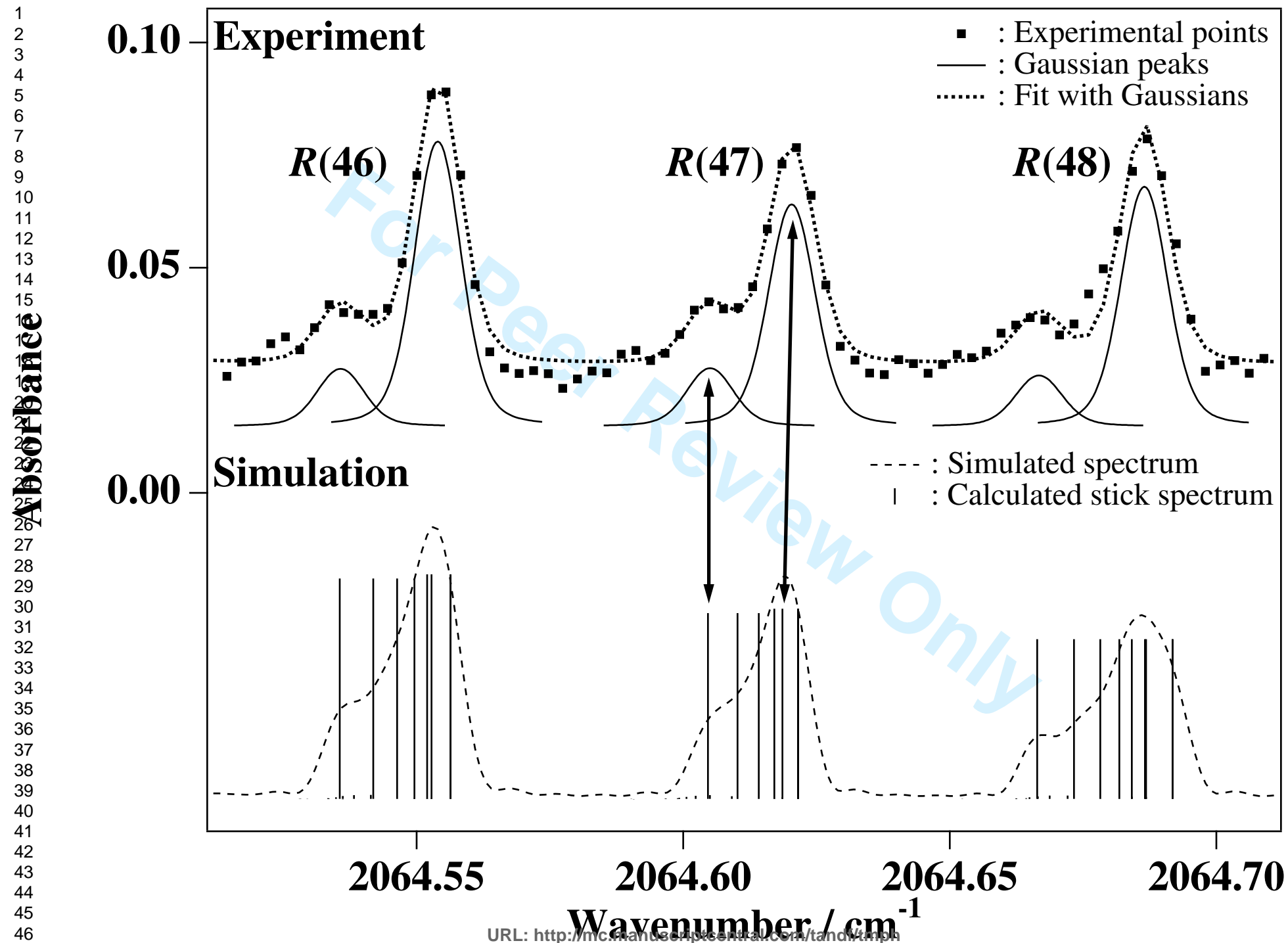
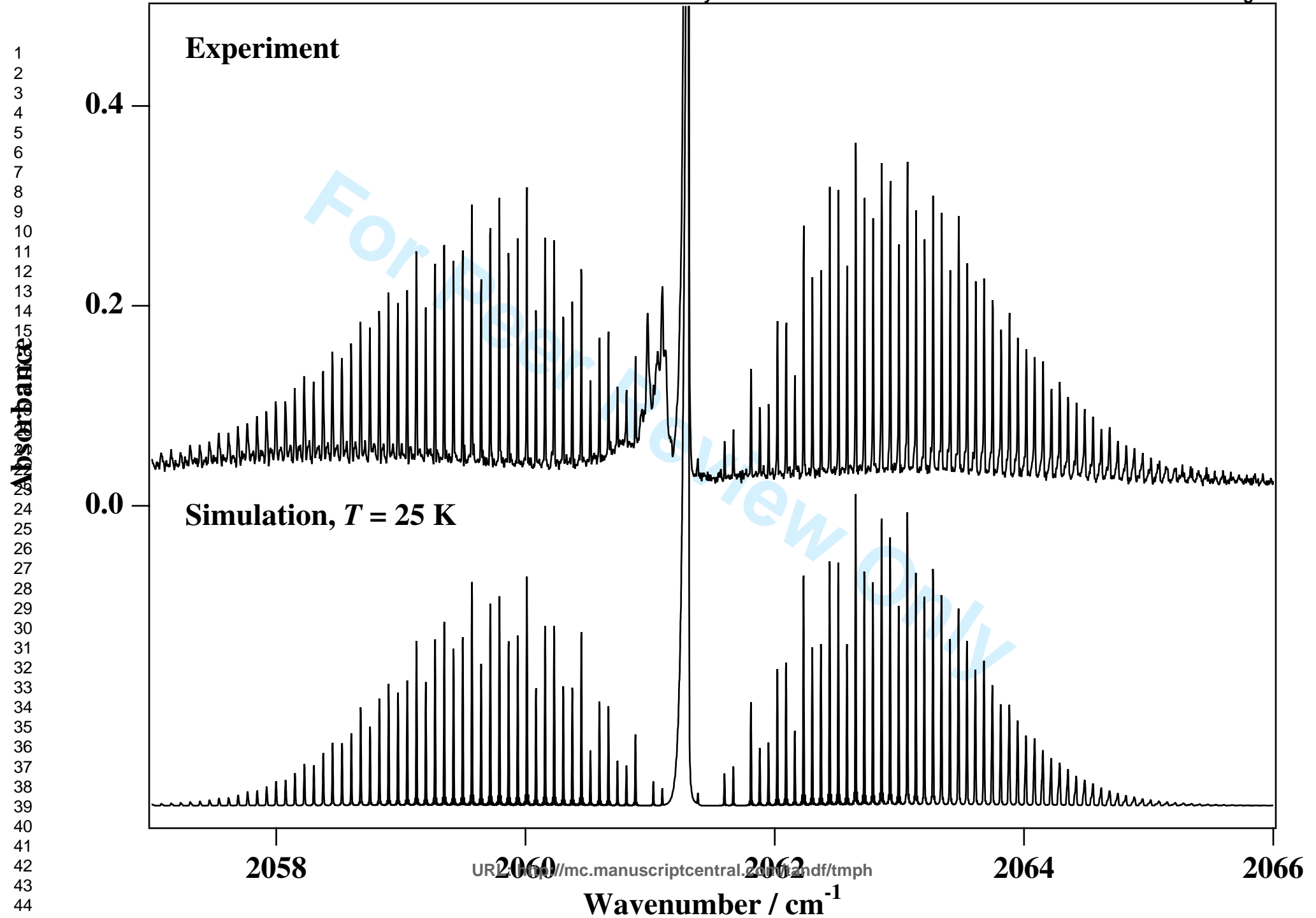


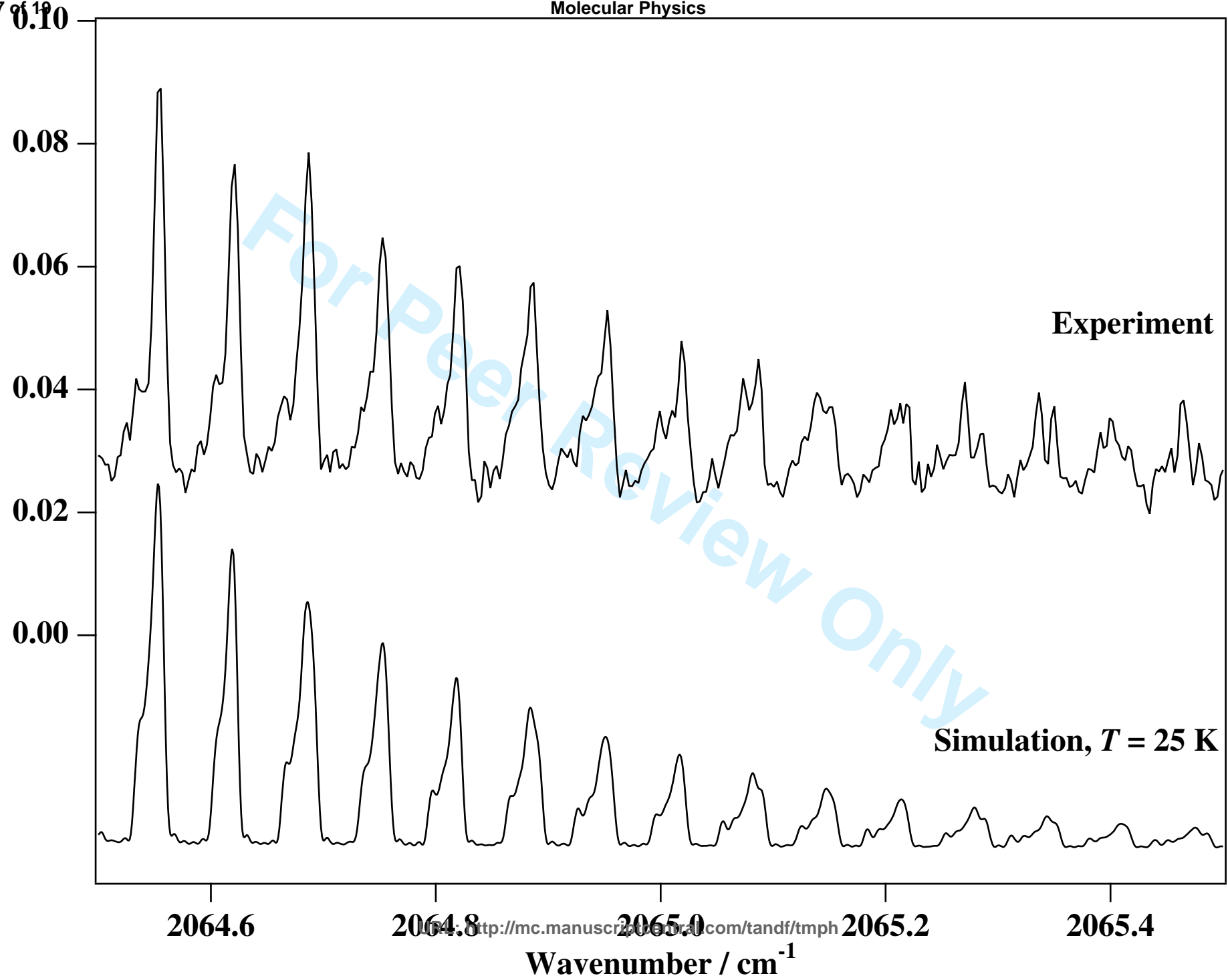
Fig. 5



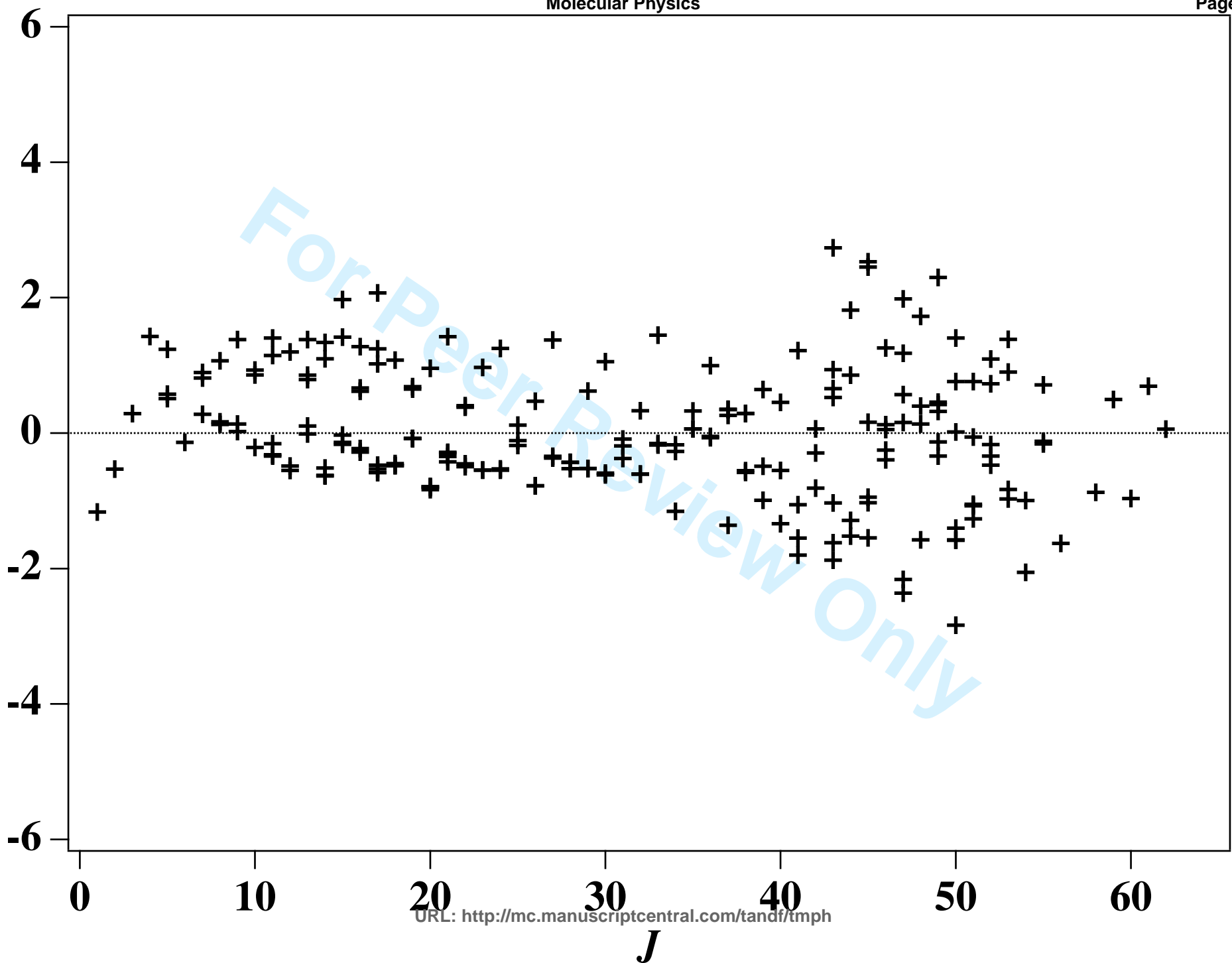




1
2
3
4
5
6
7
8
9
10
11
12
13
14
15
16
17
18
19
20
21
22
23
24
25
26
27
28
29
30
31
32
33
34
35
36
37
38
39
40
41
42
43
44
45



1
2
3
4
5
6
7
8
9
10
11
12
13
14
15
16
17
18
19
20
21
22
23
24
25
26
27
28
29
30
31
32
33
34
35
36
37
38
39
40
41
42
43
44
45



J

1
2
3
4
5
6
7
8
9
10
11
12
13
14
15
16
17
18
19
20
21
22
23
24
25
26
27
28
29
30
31
32
33
34
35
36
37
38
39
40
41
42
43
44
45
46
47
48
49
50
51
52
53
54
55
56
57
58
59
60

2061.3

2061.2

2061.1

2061.0

2060.9

